Micro- to Nanoscale Structure of Biocompatible PLA−PEO−PLA Hydrogels

Sarvesh K. Agrawal,[†] Naomi Sanabria-DeLong,[‡] Pete R. Jemian,[§] Gregory N. Tew,[‡] and Surita R. Bhatia*,[†]

Department of Chemical Engineering, University of Massachusetts, Amherst, 686 North Pleasant Street, Amherst, Massachusetts 01003, Department of Polymer Science and Engineering, University of Massachusetts, Amherst, 120 Governors Drive, Amherst, Massachusetts 01003, and Frederick Seitz Materials Research Laboratory, University of Illinois at Urbana-Champaign, Urbana, Illinois 61801

Received November 21, 2006. In Final Form: February 1, 2007

We observe large-scale structures in hydrogels of poly(L-lactide)−poly(ethylene oxide)−poly(L-lactide) (PLLA−PEO−PLLA) ranging in size from a few hundred nanometers to several micrometers. These structures are apparent through both ultra-small angle scattering (USAS) techniques and confocal microscopy. The hydrogels showed power law scattering in the USAS regime, which is indicative of scattering from fractal structures. The fractal dimension of the scattering from hydrogels revealed that the gels have large size aggregates with a mass fractal structure over the nanometer-to-micrometer length scales. The aggregates also seem to become more "dense" with an increase in the molecular weight of crystalline PLLA domains. Visualization through confocal microscopy confirms that the gels have a microstructure of interspersed micrometer-sized polymer inhomogeneities with water channels running between them. The presence of micrometer-sized water channels in the hydrogels has very important implications for biomedical applications.

Introduction

Hydrogels have generated a great deal of interest in recent years for possible applications in drug delivery[1,2] and as cell scaffolds for tissue engineering.[3−6] These materials match body tissues in interfacial tension, water content, and mechanical properties (i.e., soft and rubbery). The structure of these gels has been considered of primary importance for controlling various properties that are important for biomedical applications. Specifically, the nanometer-scale structure of the gels directly impacts their mechanical properties, whereas the structure on the micrometer length scale and microscale porosity affects cell seeding, cell motility, immunoprotective capabilities, and transport into and out of the hydrogel.[7] Additionally, the pore structure of gels is a crucial factor affecting the foreign body response that an implanted biomaterial elicits. Vascularization in and around implanted scaffolds has also been found to be strongly dependent on the implant microstructure as characterized by its pore size.[8−13] These studies establish that micrometer-sized porosity in implanted grafts or membranes leads to stable and enhanced vascularization in the system, irrespective of the chemical composition of the scaffolds.

We report here the structure of triblock copolymers of poly(L-lactide)−poly(ethylene oxide)−poly(L-lactide) (PLLA−PEO−PLLA) that form stiff gels when added to water at concentrations as low as 16 wt %. Copolymers of poly (ethylene glycol) (PEG) and poly(lactide) (PLA) with AB and ABA architecture have been extensively studied for biomedical applications.[14−27] We

* To whom correspondence should be addressed. E-mail sbhatia@ecs.umass.edu.

[†] Department of Chemical Engineering, University of Massachusetts.

[‡] Department of Polymer Science and Engineering, University of Massachusetts.

[§] University of Illinois at Urbana-Champaign.

(1) San Román, J.; Reis, R. L. *Biodegradable systems in tissue engineering and regenerative medicine*. CRC Press: Boca Raton, 2005; p 568.

(2) Yaszemski, M. J. *Tissue engineering and novel delivery system*. Marcel Dekker: New York, 2004; pp vii and 645.

(3) Drury, J. L.; Mooney, D. J. Hydrogels for tissue engineering: scaffold design variables and applications. *Biomaterials* **2003**, *24* (24), 4337−4351.

(4) Hoffman, A. S. Hydrogels for biomedical applications. *Adv. Drug Delivery Rev.* **2002**, *54* (1), 3−12.

(5) Langer, R.; Peppas, N. A. Advances in biomaterials, drug delivery, and bionanotechnology. *AIChE J.* **2003**, *49* (12), 2990−3006.

(6) Lee, K. Y.; Mooney, D. J. Hydrogels for tissue engineering. *Chem. Rev.* **2001**, *101* (7), 1869−1879.

(7) Sieminski, A. L.; Gooch, K. J. Biomaterial-microvasculature interactions. *Biomaterials* **2000**, *21* (22), 2233−2241.

(8) Brauker, J. H.; Carrbrendel, V. E.; Martinson, L. A.; Crudele, J.; Johnston, W. D.; Johnson, R. C. Neovascularization of Synthetic Membranes Directed by Membrane Microarchitecture. *J. Biomed. Mater. Res.* **1995**, *29* (12), 1517−1524.

(9) Menger, M. D.; Walter, P.; Hammersen, F.; Messmer, K. Quantitative-Analysis of Neovascularization of Different Ptfe-Implants. *European Journal of Cardio-Thoracic Surgery* **1990**, *4* (4), 191−196.

(10) Salzmann, D. L.; Kleinert, L. B.; Berman, S. S.; Williams, S. K. The effects of porosity on endothelialization of ePTFE implanted in subcutaneous and adipose tissue. *J. Biomed. Mater. Res.* **1997**, *34* (4), 463−476.

(11) Sharkawy, A. A.; Klitzman, B.; Truskey, G. A.; Reichert, W. M. Engineering the tissue which encapsulates subcutaneous implants.1. Diffusion properties. *J. Biomed. Mater. Res.* **1997**, *37* (3), 401−412.

(12) Sharkawy, A. A.; Klitzman, B.; Truskey, G. A.; Reichert, W. M. Engineering the tissue which encapsulates subcutaneous implants. II. Plasma-tissue exchange properties. *J. Biomed. Mater. Res.* **1998**, *40* (4), 586−597.

(13) Sharkawy, A. A.; Klitzman, B.; Truskey, G. A.; Reichert, W. M. Engineering the tissue which encapsulates subcutaneous implants. III. Effective tissue response times. *J. Biomed. Mater. Res.* **1998**, *40* (4), 598−605.

(14) Choi, S. K.; Kim, D. Drug-releasing behavior of MPEG/PLA block copolymer micelles and solid particles controlled by component block length. *J. Appl. Polym. Sci.* **2002**, *83* (2), 435−445.

(15) Jeong, B.; Bae, Y. H.; Lee, D. S.; Kim, S. W. Biodegradable block copolymers as injectable drug-delivery systems. *Nature (London)* **1997**, *388* (6645), 860−862.

(16) Jeong, B.; Kibbey, M. R.; Birnbaum, J. C.; Won, Y. Y.; Gutowska, A. Thermogelling biodegradable polymers with hydrophilic backbones: PEG-g-PLGA. *Macromolecules* **2000**, *33* (22), 8317−8322.

(17) Kissel, T.; Li, Y. X.; Unger, F. ABA-triblock copolymers from biodegradable polyester A-blocks and hydrophilic poly(ethylene oxide) B-blocks as a candidate for in situ forming hydrogel delivery systems for proteins. *Adv. Drug Delivery Rev.* **2002**, *54* (1), 99−134.

(18) Kricheldorf, H. R.; Meierhaack, J. Polylactones. 22. Aba Triblock Copolymers of L-Lactide and Poly(Ethylene Glycol). *Makromol. Chem.* **1993**, *194* (2), 715−725.

(19) Kubies, D.; Rypacek, F.; Kovarova, J.; Lednicky, F. Microdomain structure in polylactide-block-poly(ethylene oxide) copolymer films. *Biomaterials* **2000**, *21* (5), 529−536.

(20) Li, S. M.; Rashkov, I.; Espartero, J. L.; Manolova, N.; Vert, M. Synthesis, characterization, and hydrolytic degradation of PLA/PEO/PLA triblock copolymers with long poly(L-lactic acid) blocks. *Macromolecules* **1996**, *29* (1), 57−62.

10.1021/la063390x CCC: $37.00
Published on Web 03/31/2007

have previously reported the mechanical properties, drug release characteristics, and nanoscale structure of hydrogels formed from both PLLA−PEO−PLLA, which has crystalline hydrophobic domains, and triblocks synthesized using *meso*- or DL-lactide, which have amorphous hydrophobic domains.[28−32] We find that changes in block length and crystallinity of the hydrophobic PLA block significantly affect the structure and properties of the hydrogels formed.[33] Triblock copolymers made from crystalline lactide blocks form gels with elastic moduli that are orders of magnitude higher than the corresponding polymers from amorphous lactide blocks with similar molecular weights. Also, the elastic modulus of the hydrogels was seen to increase monotonically with an increase in the molecular weight of the crystalline PLA block.[29] The difference in mechanical properties can be attributed to the difference in nanoscale structure of the gels formed by the these systems.[34] In order to probe micrometer-scale structures in these hydrogels, scattering with larger wavelengths (e.g., with visible light or smaller angles) can be used. Since many systems that have micrometer-sized domains are opaque to visible light, ultra-small angle scattering (USAS) techniques using X-ray or neutrons are often employed. Comprehensive reviews have been published which cover the use of USAS techniques to probe structures of colloidal crystal[35] composites, geomaterial[36] polymer solutions, gels, and glasses.[37] Of these studies, very few have examined ultra-small angle scattering on gel systems. These include studies on poly(styrene)−poly(acrylic acid) (PS−PAA) gels,[38] sulfonated polystyrene gels,[39] poly(vinyl alcohol) gels,[40] poly(*N*-isopropylacrylamide) gels,[41] and gels of diblock copolypeptides.[42]

In this work, we report the micrometer-scale structures of PLA−PEO−PLA hydrogels with crystalline PLLA endblocks using USAXS/USANS and confocal microscopy techniques. The change in gel structure with the length of crystalline PLA block was studied. All the polymer gels showed excess power law scattering at low q in the USAS regime, suggesting the presence of hierarchical structures with sizes ranging from nano- to microscale. This observation was confirmed by confocal microscopy, which showed micrometer-sized polydispersed aggregates with water channels in between them in the gels. The nano- to microscale porosity of the gels, combined with their tunable mechanical properties, makes these materials excellent candidates for tissue-engineering applications.

Table 1. Characteristics of PLA−PEO−PLA Triblock Copolymers Synthesized

PLA−PEO−PLA Triblocks			
sample name	DP_{PLA}	DP_{PEO}	M_n
58L	58(PLLA)	202	13.0k
62L	62(PLLA)	202	13.3k
72L	72(PLLA)	202	14.1k
77L	77(PLLA)	202	14.4k
87L	87(PLLA)	202	15.2k

Materials and Methods

Materials. L-Lactide ((3*S*)-*cis*-3,6-dimethyl-1,4-dioxane-2,5-dione)) from Aldrich was purified by recrystallization in ethyl acetate and then sublimated prior to polymerization. The α,ω-dihydroxy poly(ethylene glycol) macroinitiator with molecular weight 8000 (PEG 8K, Aldrich) was dried at room temperature under vacuum for 2 days prior to polymerization. MALDI-TOF and GPC showed this polymer to be 8900 in weight. Stannous octanoate (Alfa Aesar) was used without further purification.

Synthesis of PLLA−PEO−PLLA Triblock Copolymer. PLLA−PEO−PLLA triblock copolymers were synthesized in the bulk. PEO was weighed into a dry round-bottom flask, purged with nitrogen, and placed into an oil bath at 150 °C. Stannous octanoate was introduced to the molten PEO, followed by the immediate addition of L-lactide to the macroinitiator/catalyst melt. The flask was capped and allowed to polymerize for 24 h at 150 °C while stirring and is then stopped by quenching in methanol. The product was dissolved in tetrahydrofuran and precipitated in a mixture of cyclohexane and *n*-hexane four times. The copolymer was then dried under vacuum for 2 days.

The polymer series that we used in our study are listed in Table 1. The sample names indicate the total length of PLA block followed by a letter indicating the stereospecificity of the PLA block, e.g., 58L refers to the polymer $PLA_{29}PEO_{202}PLA_{29}$, which is made using semicrystalline PLLA.

Sample Preparation. In a typical method of sample preparation, nanopure water for USAXS and confocal microscopy experiments or D_2O for USANS experiments was first added to a required amount

(21) Li, Y. X.; Kissel, T. Synthesis and Properties of Biodegradable Aba Triblock Copolymers Consisting of Poly(L-Lactic Acid) or Poly(L-Lactic-Co-Glycolic Acid) a-Blocks Attached to Central, Poly(Oxyethylene) B-Blocks. *J. Controlled Release* **1993**, *27* (3), 247−257.

(22) Li, Y. X.; Volland, C.; Kissel, T. In-Vitro Degradation and Bovine Serum-Albumin Release of the Aba Triblock Copolymers Consisting of Poly(L(+)Lactic Acid), or Poly(L(+)Lactic Acid-Co-Glycolic Acid) a-Blocks Attached to Central Polyoxyethylene B-Blocks. *J. Controlled Release* **1994**, *32* (2), 121−128.

(23) Liu, L.; Li, C. X.; Liu, X. H.; He, B. L. Micellar formation in aqueous milieu from biodegradable triblock copolymer polylactide/poly(ethylene glycol)/polylactide. *Polym. J.* **1999**, *31* (10), 845−850.

(24) Molina, I.; Li, S. M.; Martinez, M. B.; Vert, M. Protein release from physically crosslinked hydrogels of the PLA/PEO/PLA triblock copolymer-type. *Biomaterials* **2001**, *22* (4), 363−369.

(25) Rashkov, I.; Manolova, N.; Li, S. M.; Espartero, J. L.; Vert, M. Synthesis, characterization, and hydrolytic degradation of PLA/PEO/PLA triblock copolymers with short poly(L-lactic acid) chains. *Macromolecules* **1996**, *29* (1), 50−56.

(26) Saito, N.; Okada, T.; Horiuchi, H.; Murakami, N.; Takahashi, J.; Nawata, M.; Ota, H.; Nozaki, K.; Takaoka, K. A biodegradable polymer as a cytokine delivery system for inducing bone formation. *Nat. Biotechnol.* **2001**, *19* (4), 332−335.

(27) Yasugi, K.; Nagasaki, Y.; Kato, M.; Kataoka, K. Preparation and characterization of polymer micelles from poly(ethylene glycol)-poly(D,L-lactide) block copolymers as potential drug carrier. *J. Controlled Release* **1999**, *62* (1−2), 89−100.

(28) Agrawal, S. K.; Sanabria-DeLong, N.; Tew, G. N.; Bhatia, S. R., Novel drug release profiles from micellar solutions of PLA-PEO-PLA triblock copolymers. *J. Controlled Release* **2006**, *112* (1), 64−71.

(29) Aamer, K. A.; Sardinha, H.; Bhatia, S. R.; Tew, G. N. Rheological studies of PLLA-PEO-PLLA triblock copolymer hydrogels. *Biomaterials* **2004**, *25* (6), 1087−1093.

(30) Tew, G. N.; Sanabria-DeLong, N.; Agrawal, S. K.; Bhatia, S. R. New properties from PLA-PEO-PLA hydrogels. *Soft Matter* **2005**, *1* (4), 253−258.

(31) Agrawal, S. K.; Sardhina, H. A.; Aamer, K. A.; Sanabria-DeLong, N.; Bhatia, S. R.; Tew, G. N. Triblock PLLA-PEO-PLLA hydrogels: Structure and mechanical properties. *Polymeric Drug Delivery II: Polymeric Matrices and Drug Particle Engineering* **2006**, *924*, 102−119.

(32) Agrawal, S. K.; Sanabria-DeLong, N.; Tew, G. N.; Bhatia, S. R. Rheological Characterization of Biocompatible Associative Polymer Hydrogels with Crystalline and Amorphous Endblocks. *J. Mater. Res.* **2006**, *21*, 2118−2125.

(33) Sanabria-DeLong, N.; Agrawal, S. K.; Bhatia, S. R.; Tew, G. N. Controlling hydrogel properties by crystallization of hydrophobic domains. *Macromolecules* **2006**, *39* (4), 1308−1310.

(34) Agrawal, S. K.; Sanabria-DeLong, N.; Tew, G. N.; Bhatia, S. R., Structural Characterization of PLA-PEO-PLA Solutions and Hydrogels. 2006, In preparation.

(35) Harada, T.; Matsuoka, H. Ultra-small-angle X-ray and neutron scattering study of colloidal dispersions. *Curr. Opin. Colloid Interface Sci.* **2004**, *8* (6), 501−506.

(36) Schaefer, D. W.; Agamalian, M. M. Ultra-small-angle neutron scattering: a new tool for materials research. *Curr. Opin. Solid State Mater. Sci.* **2004**, *8* (1), 39−47.

(37) Bhatia, S. R. Ultra-small-angle scattering studies of complex fluids. *Curr. Opin. Colloid Interface Sci.* **2005**, *9* (6), 404−411.

(38) Crichton, M.; Bhatia, S. Structure and intermicellar interactions in block polyelectrolyte assemblies. *J. Appl. Crystallogr.* **2003**, *36*, 652−655.

(39) Li, Y. J.; Peiffer, D. G.; Chu, B., Long-Range Inhomogeneities in Sulfonated Polystyrene Ionomers. *Macromolecules* **1993**, *26* (15), 4006−4012.

(40) Takeshita, H.; Kanaya, T.; Nishida, K.; Kaji, K.; Takahashi, T.; Hashimoto, M. Ultra-small-angle neutron scattering studies on phase separation of poly(vinyl alcohol) gels. *Phys. Rev. E* **2000**, *61* (2), 2125−2128.

(41) Koizumi, S.; Annaka, M.; Borbely, S.; Schwahn, D. Fractal structures of a poly(N-isopropylacrylamide) gel studied by small-angle neutron scattering over a Q-range from 10(-5) to 0.1 angstrom(-1). *Physica B* **2000**, *276*, 367−368.

(42) Pakstis, L. M.; Ozbas, B.; Hales, K. D.; Nowak, A. P.; Deming, T. J.; Pochan, D. Effect of chemistry and morphology on the biofunctionality of self-assembling diblock copolypeptide hydrogels. *Biomacromolecules* **2004**, *5* (2), 312−318.

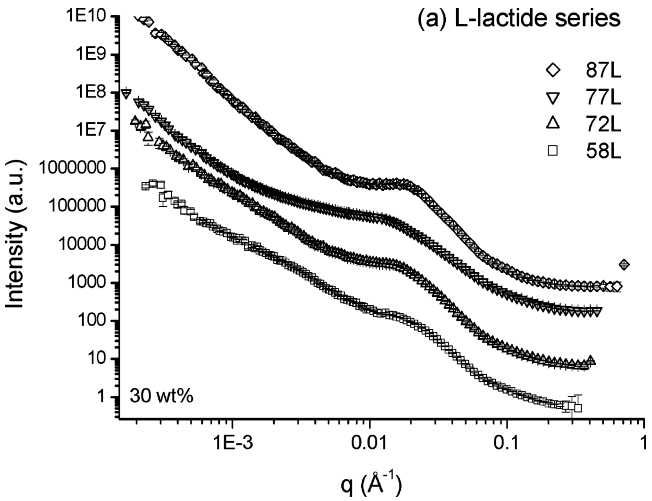

Figure 1. USAXS spectra for the L-lactide series polymers gels at 30 wt % concentration in water. The data clearly shows power law behavior in the low q regime exhibited by all the gels.

of polymer to make a solution of known concentration. The sample was then heated at 80 °C for 20 h and subsequently kept for 1−2 days at room temperature to allow for equilibration. For imaging experiments, a small amount of the fluorescent hydrophobic dye, Rhodamine (R110, Molecular Probes) was prepared in nanopure water and a drop of the solution was added to the prepared hydrogel. This sample was again allowed to sit in the dark for approximately 1 day to allow for homogeneous dispersion of the dye in the gel matrix. The polymer concentration of samples used for microscopy and USANS was 25 wt %, and for USAXS experiments, it was 30 wt %.

Ultra-small Angle X-ray Scattering (USAXS), Ultra-small Angle Neutron Scattering (USANS), and Laser Scanning Confocal Microscopy (LSCM). USAXS experiments were performed on the hydrogel samples at the UNICAT facility (sector 33-ID) of the Advanced Photon Source at Argonne National Labs. The USAXS instrument is a Bonse-Hart type diffractometer and can be used to collect scattering data over a q range of 10^{-4} to 10 Å^{-1}. The gel samples were transferred to a sample holder which provided a 1 mm path length for the X-ray beam through the sample. Extreme care was taken not to introduce any air bubbles in the hydrogel samples, and any air bubbles in the beam path were avoided by suitably positioning the sample with the help of a camera.

USANS experiments were performed on the perfect crystal diffractometer on beam port BT-5 at the National Centre for Neutron Research, NIST, Gaithersburg, MD. Preformed gel samples were transferred to a sample holder which provided a 1 mm path length for the neutron beam. The USANS data were collected on the sample for approximately 3 h over a q range of 10^{-5} to 10^{-3} Å^{-1}. The q range provided by USANS gives further insight into the gel structure over sizes which are an order of magnitude larger than seen by USAXS experiments. It also overlaps with size scales that can be visualized by confocal microscopy, thus providing scope for direct comparison of the results through the two techniques.

Imaging of the hydrogel matrix was done using a Leica microscope. Excitation of the hydrophobic dye was done at the wavelength of 488 nm. Several two-dimensional slices of the hydrogel were taken along the z-axis and were compiled to obtain information about the three-dimensional morphology of the hydrogel. *ImageJ* software was used to further obtain quantitative information about particle size distribution from the micrographs.

Results and Discussion

USAS Experiments. Ultra-small angle X-ray scattering spectra for the PLLA−PEO−PLLA gels at 30 wt % concentration are shown in Figure 1. The spectra clearly reveal structure present in the gels over two different length scales. Over the nanometer

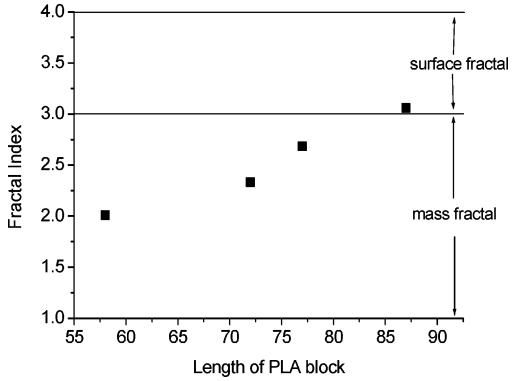

Figure 2. Power law exponents (γ) obtained from the fit of the equation $I(q) = I(0)q^{-\gamma}$ to the low q scattering spectra of the polymer gels.

length scales (∼0.01 Å^{-1} to 1 Å^{-1}), the hydrogels display a broad shoulder followed by a power law scattering regime. We have confirmed earlier that PLLA domains in the polymer are crystalline even in the hydrogel state.[33] Thus, it is expected that PLLA−PEO−PLLA polymers form nonspherical aggregates with PEO chains attached on the surface of PLLA lamellae as opposed to the flowerlike micellar aggregates which are expected to be formed by ABA triblock copolymers in a solvent selective for the midblock. At high concentrations, the polymer aggregates associate with each other, leading to formation of stiff gels. The random orientation and possible polydispersity of the nonspherical aggregates lead to formation of the broad shoulder representing a broad polydispersity in correlation lengths, at $q \approx 0.02$ Å^{-1}. We have performed complementary SANS measurements and analysis of scattering data to elucidate the micellar structure in greater detail; this will appear in a forthcoming publication. Here, we focus on the gel structure at length scales larger than ∼100 nm.

The scattering spectra show a power law behavior in the low q regime (∼10^{-4} Å^{-1} to 10^{-2} Å^{-1}), indicating the presence of micrometer-sized structures in the gel (Figure 1). This observation of large-scale structures in the gel follows very well with our understanding that association between the nanoscale micellar aggregates occurs, which leads to a network formation and gelation in these systems. This may be similar in nature to the observation of large-scale structures in other associative network systems.[43] The gel structure can be envisaged as a cross-linked network of aggregates with water channels running in between them[42] and dimensions from nano- to micrometer scale. The spectra at low q can be fit to a power law, $I(q) = I(0)q^{-\gamma}$, and the values of the exponent γ are given in Figure 2. The value of the exponents is seen to vary in the range 2−3 for all the gels.

Power law scattering behavior is often indicative of scattering from fractal structures.[38,44] These can be either mass or surface fractals, and both can be found in polymeric systems. For a mass fractal, the mass M is directly proportional to some fractional power d_f of the radius. The power law exponent d_f, called the fractal dimension, is indicative of the "openness" of the fractal structure. For mass fractals, this exponent can vary from 1 for a loosely connected aggregate with ill-defined interfaces to 3 for a very dense aggregate structure. Surface fractals are compact structures but have a surface area, A, that is proportional to some fractional power, d_s, of the radius. For objects which are surface

(43) Loizou, E.; Butler, P.; Porcar, L.; Kesselman, E.; Talmon, Y.; Dundigalla, A.; Schmidt, G. Large scale structures in nanocomposite hydrogels. *Macromolecules* **2005**, *38* (6), 2047−2049.

(44) Schmidt, P. W. Small-Angle Scattering Studies of Disordered, Porous and Fractal Systems. *J. Appl. Crystallogr.* **1991**, *24*, 414−435.

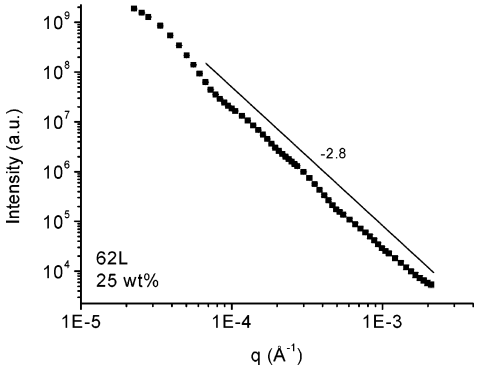

Figure 3. USANS spectra for 62L polymer gel at 25 wt % concentration. The spectra shows presence of large scale aggregates in the gel over a size range of ~0.5−30 μm, which is 1 order of magnitude larger than that observed through USAXS.

fractals, d_s varies from 3 for very rough surfaces to 2 for scattering from smooth surfaces. Summarizing mathematically

$$M \sim R^{d_f} \quad 1 < d_f < 3 \quad \text{mass fractals}$$

$$A \sim R^{d_s} \quad 2 < d_s < 3 \quad \text{surface fractals}$$

is the defining relation for mass and surface fractals. The scattering exponent (γ) is equal to d_f for mass fractals and varies from 1 to 3, whereas it is equal to $6 - d_s$ for surface fractals and varies from 3 to 4. On the basis of the above description, it can be deduced that the hydrogel structure becomes denser as the molecular weight of the PLLA chains is increased.

A Guinier scattering region was not seen at low q values in the USAXS regime, indicating that micrometer-sized aggregates with sizes larger than that probed by USAXS could be present in the gels. A USANS experiment was thereby performed on a 25 wt % hydrogel sample of one of the polymers, 62L, in order to obtain information about the gel microstructure over the q range of ~2.3×10^{-3} to 2.3×10^{-5} Å^{-1}, corresponding to length scales of roughly 0.28 to 28 μm. Power law scattering was again observed for the hydrogel over the whole q range, with no Guinier regime present (Figure 3) similar to the USAXS spectra. The power law exponent of the USANS spectra is 2.8, which is larger than that observed for the hydrogel of the 58L sample at 30 wt % through USAXS (Figure 2). The value of the fractal dimension, however, is still seen to be in the range observed for other polymer hydrogels. The hydrogels thus appear to have a fractal-like structure with aggregates much larger than 30 μm.

Confocal Microscopy. For further insight into the hierarchical structure in the hydrogel, we performed confocal microscopy on the hydrogels of PLLA−PEO−PLLA copolymers. Figure 4 shows representative fluorescence micrographs of 25 wt % hydrogel of 58L, 72L, and 87L. The micrographs clearly show large-scale aggregates in the size range 1−80 μm for all the polymers. The information obtained through microscopy confirms the conclusions about the gel microstructure as derived though USAS. The brighter spots in the micrographs indicate the regions where the hydrophobic fluorescent dye preferentially segregates, which are most likely to be the regions where polymer aggregates are formed or regions rich in polymer. The darker regions in the image show regions with water-filled channels and pores or regions poor in polymer concentration, thereby showing that a substantial amount of water is present in the gel matrix. Thus, the micrographs show that the hydrogels consist of interspersed inhomogeneous polymer aggregates with water channels running between them. This can have important implications for drug

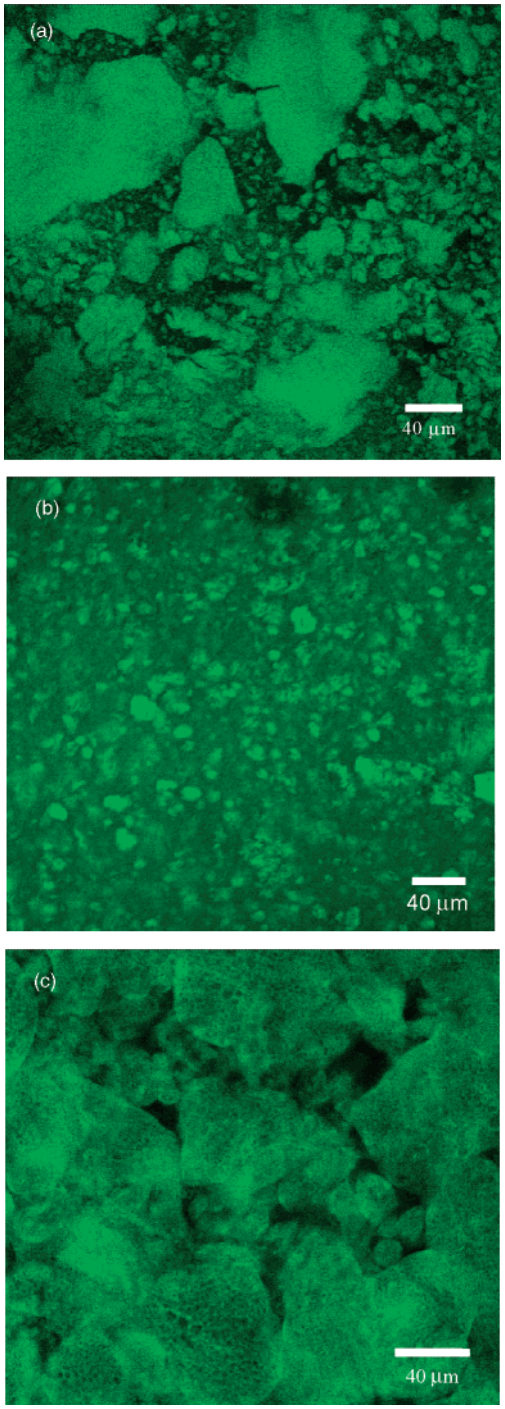

Figure 4. Confocal images of the (a) 58L, (b) 72L, and (c) 87L polymer gels at 25 wt % concentration. The gels were stained by Rhodamine dye as fluorescent probes. The micrographs clearly show the presence of micrometer-sized polydispersed aggregates of the polymer which are preferentially stained by the dye. The black regions in the picture are micrometer-sized pores and water channels which run throughout the gel matrix.

delivery and tissue-engineering applications, because the presence of water channels facilitates transport of drugs, nutrients, or cells into and out of the matrix.[7] Also, as discussed earlier, porosity of scaffolds on micrometer length scales has been found to be the primary factor responsible for growth of vasculature through the system, again suggesting the utility of these materials for tissue engineering.[8−13] Similar large-scale inhomogenities and water pores have also been observed for copolypeptide hydrogels,[42] PS−PAA hydrogels,[45] and polymer nanocomposite

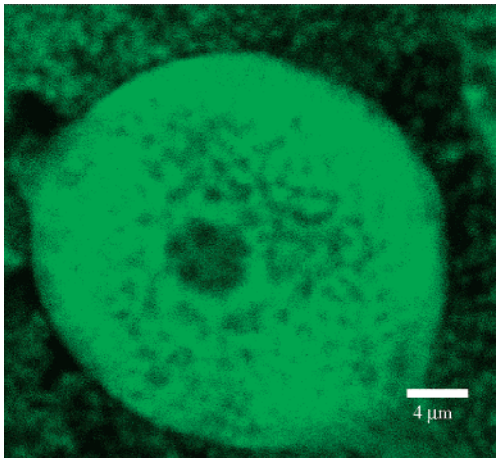

Figure 5. Magnified image of an aggregate in 87L polymer gel at 25 wt % concentration. The micrograph shows that the aggregate has a cagelike network structure. The image also shows sub-micrometer-sizef porosity in the aggregates.

hydrogels.[43] Another noticeable feature in the images obtained for the 87L polymers is that some aggregates have a cagelike interconnected structure. A closeup of this cagelike structure (Figure 5) shows that the features forming the "cage" are close to 1 μm in size. This indicates that the individual aggregates also have a highly porous networked structure with a smaller dimension, indicating that these gels have water channels with dimensions spanning less than 1 μm to several micrometers in length scale.

To further quantify our observations, image analysis was performed on the optical micrographs using *ImageJ* software. The micrographs were segmented into dark and white regions, representing aggregates and water channels, respectively. The area of the aggregates was then determined and a distribution of aggregate sizes generated. Since the aggregates are randomly shaped, the square root of the area of the aggregates was taken as the characteristic size. The resulting aggregate size distributions are shown in Figure 6 for two gels 58L and 72L. The abscissa of the graphs has been cut off at 12 μm for both cases, because the majority of the aggregates lie in this size range, even though a few aggregates of very large sizes (up to 120 μm) can be clearly seen in the images. The statistics of the distribution are shown in Table 2. Even though the average aggregate sizes fall around 2−3 μm, the distributions are clearly skewed toward smaller sizes, and hence the median and mode are a more representative measure of the aggregate sizes. These range from 0.8 to 1.7 μm. Aggregates smaller than 0.5 μm are likely present in these gels, which give a power law scattering in the USAS regime; however, smaller aggregates cannot be observed via confocal microscopy. In Table 2, we also report the values of τ, which characterizes the number distribution of aggregates with mass of aggregates according to the equation $N(M) \sim M^{-\tau}$. The relevance of this parameter is described further below.

Polydispersity Effects on the Fractal Dimension. For all the polymers, the number distribution of the aggregates was seen to have a power law dependence on the aggregate size, which in turn can be related to the aggregate mass as $M \sim R^{d_f}$, where d_f is the mass fractal dimension of the aggregate and is 3 for a surface fractal object. It has been observed by other researchers that for polydisperse systems the scattering exponent (γ) may depend on both the fractal dimension and the polydispersity

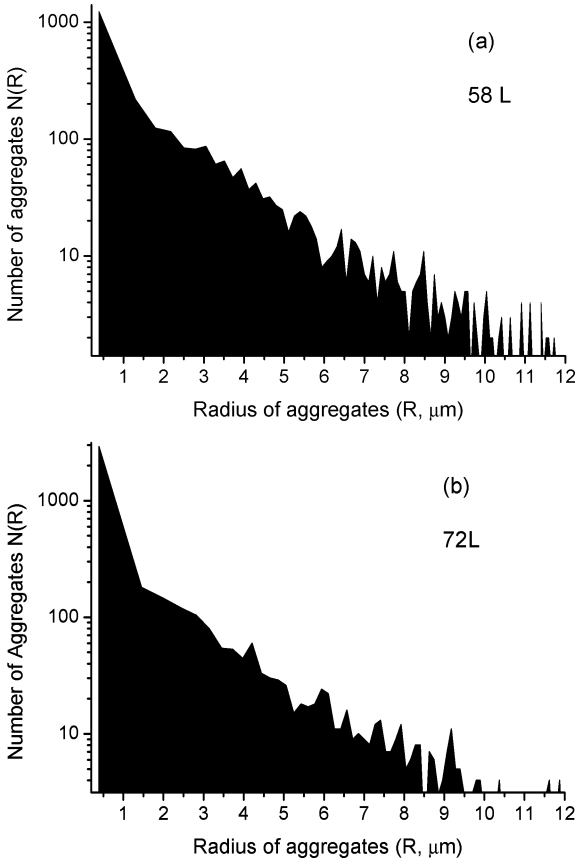

Figure 6. Aggregate size distribution in the gels of (a) 58L and (b) 72L polymers at 25 wt % concentration. The abscissa of the graphs has been cut at 12 μm, since the majority of the aggregates lie in this size range.

Table 2. Statistics of Particle Size Distribution[a]

polymer	mean	σ	median	mode	τ
58L	2.7	2.5	1.7	0.7	1.21 ± 0.06
72L	2.0	2.4	0.8	0.8	1.07 ± 0.05

[a] All sizes are in μm.

exponent for both the surface and mass fractals.[44,46−50] For the case in which the mass number distribution of the aggregates has a power law dependence on the aggregate mass ($N(M) \sim M^{-\tau}$), the power law dependence of the scattering intensity on the scattering wave vector is calculated as[49]

$$I \sim \int M^{-\tau} I_M \, \mathrm{d}M \begin{cases} \sim q^{-d(3-\tau)} & \text{surface fractal} \\ \sim q^{-d_f(3-\tau)} & \text{mass fractal} \end{cases} \quad (1)$$

where d is the number of dimensions. Here, I_M is the scattering intensity from monodispersed objects and is given by the relation $I_M \sim M^2 F(qR)$. In the absence of interactions, $F(qR) = 1 - (qR)^2/3 + \ldots$ for $qR \ll 1$. For $qR \gg 1$, scattering from both surface and mass fractals shows a power law behavior given as $F(qr) \sim (qR)^{-\gamma}$. The integral in eq 1 is absolutely convergent

(45) Crichton, M. A.; Bhatia, S. R., Large-scale structure in gels of attractive block copolymer micelles. *Langmuir* **2005**, *21* (22), 10028−10031.

(46) Martin, J. E.; Ackerson, B. J. Static and Dynamic Scattering from Fractals. *Phys. Rev. A* **1985**, *31* (2), 1180−1182.

(47) Bale, H. D.; Schmidt, P. W. Small-Angle X-Ray-Scattering Investigation of Submicroscopic Porosity with Fractal Properties. *Phys. Rev. Lett.* **1984**, *53* (6), 596−599.

(48) Schaefer, D. W.; Martin, J. E.; Wiltzius, P.; Cannell, D. S. Fractal Geometry of Colloidal Aggregates. *Phys. Rev. Lett.* **1984**, *52* (26), 2371−2374.

(49) Martin, J. E. Scattering Exponents for Polydisperse Surface and Mass Fractals. *J. Appl. Crystallogr.* **1986**, *19*, 25−27.

(50) Martin, J. E.; Hurd, A. J. Scattering from Fractals. *J. Appl. Crystallogr.* **1987**, *20*, 61−78.

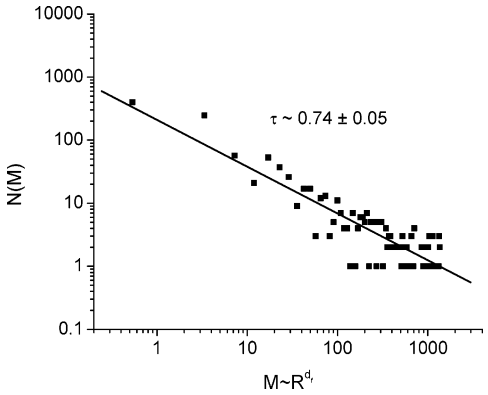

Figure 7. Power law decay of the number distribution of aggregate masses seen in hydrogel of 62L polymer.

when reasonable bounds are put on the value of τ, which are $2 < \tau < 3$ for a mass fractal and $1 + d_s/d < \tau < 3$ for a surface fractal.

In the case of systems for which the value of τ lies below these bounds, the integral in eq 1 is convergent if the number distribution has the form $N(M) \sim M^{-\tau} f(M/M_w)$ where $f(x)$ is a cutoff function which is constant for $x \ll 1$ and decays faster than a power law for $x \gg 1$. Here, M_w is the weight-averaged mass. This is also a physically important case since many real systems may have a maximum aggregate size, which is finite. For this case, a straightforward calculation for scattering intensity gives[49]

$$I\begin{cases} \sim q^{-d_f} & \tau < 2 \quad \text{mass fractal} \\ \sim q^{-2d+d_s} & \tau < 1 + \dfrac{d_s}{d} \quad \text{surface fractal} \end{cases} \tag{2}$$

Hence, for fractal structures, polydispersity in aggregate sizes becomes irrelevant in this regime, and power law scattering shows a dependence on q similar to that for monodispersed systems.

In order to ascertain if polydispersity in aggregates affects scattering in the gels, the number distribution of the aggregates was plotted against aggregate mass, and power law exponents (τ) of the dependence were obtained (Figure 7). An estimate of the mass of the aggregates was obtained by using the scaling relation $M \sim R^{d_f}$. This exercise was performed for all the samples even though 62L is the only sample for which the size scales observed by USAS and confocal microscopy overlap. The values of τ obtained for all the samples were seen to lie well within the bounds of eq 2 and are listed in Table 2. It can thus be concluded that polydispersity does not affect the fractal exponents obtained for the gels and the hydrogels have a mass fractal like structure with porosity in the network present over the nanometer to micrometer length scales.

Conclusions

We have observed the existence of large-scale structures in hydrogels of PLLA−PEO−PLLA through USAXS/USANS and microscopy and have compared the structure of hydrogels with increasing MW of crystalline PLA domains. Low q scattering from the polymer hydrogels shows a power law behavior with power law exponents less than or equal to 3. This behavior is indicative of scattering from mass fractals. The internal structure of the gels also seems to become denser as the PLLA block length is increased. Further investigation of the structure via microscopy indicates that the hydrogels are composed of polydispersed aggregates of sizes ranging from less than 1 to several micrometers. The median and mode of the aggregate and corresponding pore sizes lie in the range 0.8−1.7 μm, though a few aggregates/pores of sizes even larger than 100 μm are clearly seen in the microscopy images. The presence of micrometer-sized water channels and pores running throughout the gels could facilitate transport and cell motility and thus is an important characteristic for drug delivery and tissue-engineering applications.

Acknowledgment. This material is based upon work supported by the National Science Foundation under grant no. DMI-0531171. Support for this work was also provided by a 3M Nontenured Faculty Award and Dupont Young Professor Award to S.R.B. and a National Research Service Award, T32 GM08515, from the National Institutes of Health to N.S.D. USAXS data were taken with the help of Pete Jemian at APS. The UNICAT facility at the Advanced Photon Source (APS) is supported by the U.S. DOE under award no. DEFG02-91ER45439, through the Frederick Seitz Materials Research Laboratory at the University of Illinois at Urbana−Champaign, the Oak Ridge National Laboratory (U.S. DOE contract DE-AC05-00OR22725 with UT-Battelle LLC), the National Institute of Standards and Technology (U.S. Department of Commerce), and UOP LLC. The APS is supported by the U.S. DOE, Basic Energy Sciences, Office of Science under contract no. W-31-109-ENG-38. We acknowledge the support of the National Institute of Standards and Technology, U.S. Department of Commerce, in providing the neutron research facilities used in this work. This work also utilized central facilities of the NSF-sponsored MRSEC on Polymers (DMR-0213695).

LA063390X